

Trapped-ion Lissajous trajectories

R. F. Rossetti, G. D. de Moraes Neto, J. Carlos Egues, and M. H. Y. Moussa¹

¹*Instituto de Física de São Carlos, Universidade de São Paulo,
Caixa Postal 369, 13560-970, São Carlos, São Paulo, Brazil*

Here we present a protocol for generating Lissajous curves with a trapped ion by engineering Rashba- and the Dresselhaus-type spin-orbit interactions in a Paul trap. The unique anisotropic Rashba α_x, α_y and Dresselhaus β_x, β_y couplings afforded by our setup also enables us to obtain an “unusual” Zitterbewegung, i.e., the semiconductor analog of the relativistic trembling motion of electrons, with cycloidal trajectories in the absence of magnetic fields. We have also introduced bounded SO interactions, confined to an upper-bound vibrational subspace of the Fock states, as an additional mechanism to manipulate the Lissajous motion of the trapped ion. Finally, we accounted for dissipative effects on the vibrational degrees of freedom of the ion and find that the Lissajous trajectories are still robust and well defined for realistic parameters.

PACS numbers: 32.80.-t, 42.50.Ct, 42.50.Dv

Increasing interest in quantum simulations and controllable trapped ion systems — used through the last two decades as a staging platform to investigate fundamental quantum phenomena [1] and to implement quantum information processing [2]— have led to the emulation of the quantum relativistic wave equation. Apart from trapped ions [3, 4], a number of distinct setups have been used to simulate zitterbewegung in a variety of physical systems such as quantum wells [5], photonic crystals [6], Bose-Einstein condensates [7] and ultracold atoms [8]. It has been demonstrated that Bose-Einstein condensates can provide an analog to sonic black holes [9] and the Higgs boson [10].

In trapped-ion system Gerritsma *et al.* [11] reported a proof-of-principle quantum simulation of the one-dimensional Dirac equation within a trapped-ion experiment. Measuring the time-evolving position of a single trapped ion set to mathematically simulate a free relativistic quantum particle, they demonstrated the Dirac Zitterbewegung, as anticipated in Ref. [3], for distinct initial superpositions of positive- and negative-energy spinor-like states. The momentum-spin coupling, which naturally takes place in the relativistic quantum regime, was simulated by the laser-induced coupling between the vibrational and the electronic states of the ion.

Motivated by the exciting results in Refs. [3, 11], here we consider a single two-level atom in a two-dimensional Paul trap with four electrodes, Fig.1, and show how to obtain spin-orbit interactions of the Rashba and Dresselhaus types, ubiquitous in quantum spintronics and in emerging areas of condensed matter physics such as topological insulators and Majorana fermions. Our setup enables us to engineer Hamiltonians with *anisotropic* SO couplings such as

$$H_{SO} = \frac{\alpha_x}{\hbar} \sigma_x p_y - \frac{\alpha_y}{\hbar} \sigma_y p_x + \frac{\beta_x}{\hbar} \sigma_x p_x + \frac{\beta_y}{\hbar} \sigma_y p_y, \quad (1)$$

which generalize the canonical form of the SO interactions in semiconductor quantum wells to include distinct

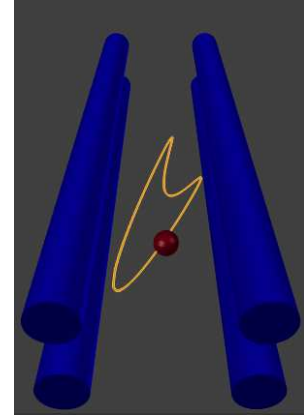


FIG. 1: The schematic of the experimental Paul trap setup illustrating the ion performing a Lissajous curve.

Rashba α_x, α_y and Dresselhaus β_x, β_y couplings. In (1) \vec{p} and $\vec{\sigma}$ denote the momentum and pseudo-spin operators, respectively, of the trapped ion. Interestingly, the anisotropic SO couplings can give rise to physical phenomena not possible in the condensed matter environment, e.g., ionic motion with trajectories following Lissajous curves, Fig.1. In Fig. 2 we show the whole set of Lissajous curves followed by the trapped ion, which we discuss in detail below. In addition, we can also obtain the “unusual” Zitterbewegung, a trembling relativistic motion, with cycloidal trajectories in the absence of magnetic fields [12]. We also demonstrate how to engineer bounded-SO Hamiltonians, confined to an upper-bound vibrational subspace of the Fock states — leading to distinct periodic motions— apart from analysing the effects of dissipation over trajectories.

Engineering the anisotropic Rashba interaction. We consider a two-level ion acted upon by two laser beams perpendicular to one another in x and y directions, each providing red and blue sidebands simultaneously via an electro-optical modulator [13]. From the four generated

frequencies ω_ℓ and relative phases ϕ_ℓ , two are tuned to the first-blue sidebands, each coming from one of the original laser beams. The other two are tuned to the first-red sidebands, leading to the Hamiltonian ($\hbar = 1$)

$$H = i [\Omega_x \eta_x (e^{i\phi_1} a_x + e^{i\phi_2} a_x^\dagger) + \Omega_y \eta_y (e^{i\phi_3} a_y + e^{i\phi_4} a_y^\dagger) \sigma_+ + H.c.], \quad (2)$$

where η_α is the Lamb-Dicke parameter and Ω_s the Rabi frequency for the coupling between the electronic (ground $|g\rangle$ and excited $|e\rangle$) states of the ion and its two-dimensional motional degrees of freedom, described by the annihilation a_s and creation a_s^\dagger operators with respect to each direction $s = x, y$. Moreover, $\sigma_+ = |e\rangle\langle g|$ and $\sigma_- = \sigma_+^\dagger$ are the raising and lowering operators for the two-level system. By adjusting $\phi_1 = 0, \phi_2 = \pi, \phi_3 = \pi/2$, and $\phi_4 = 3\pi/2$, we obtain, in the interaction picture, the anisotropic 2D Rashba SO interaction

$$H = (\Delta_x \eta_x \Omega_x p_x \sigma_y - \Delta_y \eta_y \Omega_y p_y \sigma_x), \quad (3)$$

where $p_s = i(a_s^\dagger - a_s)/2\Delta_s$, with $\Delta_s = 1/\sqrt{2m\nu_s}$, m being the ion mass and ν_s the trap frequency in the s direction. When we adjust the laser parameters so that $\Delta_x = \Delta_y$, $\eta_x = \eta_y$, and $\Omega_x = \Omega_y$, the above derived Hamiltonian reduces exactly to the usual Rashba interaction $H = \gamma(p_x \sigma_y - p_y \sigma_x)$ in quantum wells, where $\gamma = \Delta\eta\Omega$.

Interestingly, we find that a 3D trap with an additional laser beam and an appropriate set of phase constants ϕ_ℓ enables us to engineer a 3D Rashba-like term

$$H = \gamma \hat{r} \cdot (\vec{p} \times \vec{\sigma}), \quad (4)$$

where \vec{r} sets the position of the ion in relation to the trap center. Unlike the 2D and 3D cases in Eqs. (3) and (4), the 1D Rashba-like interaction $H = \gamma p_x \sigma_y$ does not lead to the unusual Zitterbewegung with cycloidal orbits. However, when one of the original laser beams leading to Eq. (2) is adjusted to produce a carrier interaction (instead of the simultaneous red and blue sidebands), we end up with the 1D interaction

$$H = \gamma p_x \sigma_y + \tilde{\Omega} \sigma_z. \quad (5)$$

Here, as in the Dirac equation, the energy gap provided by the Stark shift term $\tilde{\Omega} \sigma_z$ ($\tilde{\Omega}$ being also a Rabi frequency), is a key ingredient for producing Zitterbewegung. In addition, an appropriate choice of parameters of the laser producing simultaneous blue and red sidebands leads straightforwardly to a Hamiltonian similar to that in Eq. (5): $H = \eta\Omega\Delta_x p_x \sigma_x + \tilde{\Omega} \sigma_z$, which simulates the 1D Dirac equation [3].

Anisotropic Dresselhaus term. We can also simulate the linear Dresselhaus SO interaction by adjusting $\phi_1 = -\phi_2 = \pi/2$ and $\phi_3 = -\phi_4 = 3\pi/2$ in Eq. (2); we find

$$H = \gamma (p_x \sigma_x - p_y \sigma_y), \quad (6)$$

which, together with the Rashba coupling, is a crucial ingredient to manipulate the electron spin in quantum spintronics and, more recently, to obtain exotic topological phases of matter. We can also consider four laser beams simultaneously and hence generate a Rashba-Dresselhaus Hamiltonian as shown in Eq. (1), with $\alpha_s = \Delta_s \eta_s \Omega_s$ and $\beta_s = \Delta_s \tilde{\eta}_s \tilde{\Omega}_s$, enabling us to simulate the canonical SO interaction of quantum spintronic in our setup.

At this point it is important to stress that a four-level ion, as in Ref. [3], can also be used to engineer the interactions of the forms [Eqs. (1)–(6)]. In this case we have to consider two additional states $|g'\rangle$ and $|e'\rangle$ having the same angular momentum as $|g\rangle$ and $|e\rangle$, respectively, but distinct energies and magnetic momenta. For instance, by exciting only the crossed transitions $g \leftrightarrow e'$ and $e \leftrightarrow g'$, we can exactly simulate the mathematical structure of the Hamiltonian used to obtain the unusual Zitterbewegung in Ref. [12]. In this case, the isotropic Rashba-type interaction (3) is modified to

$$H = \tilde{\sigma}_x \otimes \Gamma (p_x \sigma_y - p_y \sigma_x), \quad (7)$$

where $\Gamma = \Delta\eta\Omega$ and $\tilde{\sigma}_x$ is the Pauli matrix in subspace $\{|g'\rangle, |e'\rangle\}$. All other Hamiltonians [Eqs. (1)–(6)] are also modified via a tensor products with $\tilde{\sigma}_x$. For simplicity, we restrict our analysis to a two-level system which, as shown below, gives rise to the same dynamics for the unusual Zitterbewegung as given in Ref. [12].

“Bounded” spin orbit interaction. Before analyzing the Lissajous curves in Fig. 2, we would like to address a case, with no analog in the solid state physics, in which an *upper-bound* interaction [14] between the internal and the vibrational degrees of freedom of the ion is engineered. Following the steps outlined in Ref. [14], we can obtain

$$H_{k=\pm 1} = \chi(\eta) [\mathbf{A}(\eta) \sigma_\pm + \mathbf{A}^\dagger(\eta) \sigma_\mp], \quad (8)$$

where $\chi(\eta) = \eta(1 - \eta^2/2)\Omega e^{i\phi}$ and $\mathbf{A}(\eta) = [1 - \eta^2 a^\dagger a/2] a$. Expanding the operators A and A^\dagger in the Fock space basis and adjusting the Lamb-Dicke parameter to $\eta^2 = 2/N$ [$\eta^2 = 2/(N-1)$ with $N \in \mathbb{Z}$] such that $\mathbf{A}^\dagger(\eta)|N\rangle = 0$ [$\mathbf{A}(\eta)|N\rangle = 0$], we find that for an initial vibrational state prepared within the *upper-bound* subspace ranging from $|0\rangle$ to $|N\rangle$, the Hamiltonian $H_{k=\pm 1}$ becomes

$$H_\pm^{(ub)} = \sum_{n=0}^{N-1} \chi_n (|n\rangle \langle n+1| \sigma_\pm + H.c.). \quad (9)$$

where $\chi_n = \sqrt{n+1}(1 - \eta^2 n/2)\chi(\eta)$. By using the Hamiltonian (1) instead of (2) we can derive all the above spin-orbit interactions but restricted to within the *upper-bound* subspace. In particular, for the case of the *upper-bound* Rashba-Dresselhaus interaction, with the same adjustment of the laser parameters as above we obtain

$$H = \alpha_x p_x^{ub} \sigma_y - \alpha_y p_y^{ub} \sigma_x + \beta_x p_x^{ub} \sigma_x - \beta_y p_y^{ub} \sigma_y, \quad (10)$$

where $p_s^{ub} = i [\mathbf{A}_s^\dagger(\eta) - \mathbf{A}_s(\eta)] / 2\Delta_s$, $\alpha_s = \chi_n \eta \Delta_s$, and $\beta_s = \tilde{\chi}_n \eta \Delta_s$. As should become clearer below, when discussing the trajectories, the bounded Hamiltonian (10) is able to generate Lissajous trajectories other than those derived from the usual Rashba-Dresselhaus interaction. It also enables Lissajous curves from an initial coherent state, which does not occur with interaction (1). We finally note that for each upper-bound parameter N we get distinct trajectories.

Cycloidal Zitterbewegung. Now let us analyze the zitterbewegung with the (anisotropic) Rashba-like coupling in Eq. (3), from which we obtain the time-dependent components of position operator

$$s(t) = s(0) - \frac{c^2 P_s}{H} t - iH \left(c\sigma_r + \frac{c^2 P_s}{H} \right) (e^{iHt} - 1), \quad (11)$$

with $r \neq s = x, y$. We note that Eq. (11) exhibits the same time dependence as that coming from the Dirac zitterbewegung, with the trembling motion arising from the third term on the right side of the equality. Hereafter we consider the initial state $|\psi(0)\rangle = \prod_s \exp[-(p_s - p_{0s})/2\mu_s] \otimes |\varphi\rangle$, with both momentum eigenstates peaked around p_{0s} (μ_s being the width of the distribution) and $|\varphi\rangle$ standing for the ionic internal state, we thus compute the mean value $\langle \bar{s}(\tau) \rangle = \text{Tr}[\bar{s}\rho(t)]$:

$$\begin{aligned} \langle \bar{s}(\tau) \rangle &= \langle \bar{s}(0) \rangle + (-1)^{1+\delta_{sx}} \varepsilon^{\delta_{sy}} \langle \sigma_r \rangle \tau \\ &+ \frac{\varepsilon \bar{p}_r}{2\xi} \left[\cos\left(2\xi^{1/2}\tau\right) - 1 \right] \langle \sigma_z \rangle \\ &+ \frac{\varepsilon \bar{p}_r}{2\xi^{3/2}} \left[\sin\left(2\xi^{1/2}\tau\right) - 2\xi^{1/2}\tau \right] \\ &\times (\langle \sigma_x \rangle \bar{p}_x + \varepsilon \langle \sigma_y \rangle \bar{p}_y) \end{aligned} \quad (12)$$

where we have defined the dimensionless position $\bar{s} = s/\Delta$, momentum $\bar{p}_s = 2\Delta p_s$ and time $\tau = \eta\Omega t$, with $\xi = \sqrt{\langle \bar{p}_s^2 \rangle + \langle \bar{p}_r^2 \rangle}$ and $\varepsilon = \Delta_x^2 \eta_x \Omega_x / \Delta_y^2 \eta_y \Omega_y$. Here δ_{sx} is the Kronecker delta and $\varepsilon = 1$ ($\neq 1$) gives the isotropic (anisotropic) Rashba-type interaction. We take the momentum state to be a distribution in the x direction with $\varepsilon^2 \bar{p}_y^2 \gg \bar{p}_x^2$ and the vacuum state in the y direction. With the internal state $|\varphi\rangle = |a\rangle |\uparrow\rangle + |b\rangle e^{i\phi} |\downarrow\rangle$, where $|a| \neq |b|$ and $\phi = \pi/2$, such that $\langle \sigma_x \rangle = 0$, we obtain

$$\langle \bar{x}(\tau) \rangle = \left(\frac{\varepsilon^2 \bar{p}_y^2}{2\bar{p}_x^2} - 1 \right) \tau - \frac{\varepsilon^2 \bar{p}_y^2}{2\bar{p}_x^3} [\sin(2\bar{p}_x \tau)], \quad (13a)$$

$$\langle \bar{y}(\tau) \rangle = \frac{\varepsilon \bar{p}_x}{2\xi} [\cos(2\bar{p}_x \tau) - 1]. \quad (13b)$$

The above equations lead to all the trochoids in Ref. [12], for appropriate parameters. When considering the Dresselhaus-type interaction (6) we obtain exactly the same time dependence as in Eq. (12) but with $\langle \sigma_x \rangle \bar{p}_x + \varepsilon \langle \sigma_y \rangle \bar{p}_y$ changed by $\langle \sigma_x \rangle \bar{p}_y + \varepsilon \langle \sigma_y \rangle \bar{p}_x$, affecting only the amplitude of the curves generated by Eq. (12).

This ensures that the cycloidal trajectories without magnetic fields, derived in Ref. ([12]) by considering the effects of an interband SO term, can also be obtained here from the anisotropic Dresselhaus interaction. However, when the Rashba- and the Dresselhaus-type interactions come together as in Eq. (1), we obtain for the isotropic case ($\alpha_x = \alpha_y$ and $\beta_x = \beta_y$)

$$\begin{aligned} \langle \bar{s}(\tau) \rangle &= \langle \bar{s}(0) \rangle + \left[(-1)^{1+\delta_{sx}} (\langle \sigma_s \rangle - \kappa \langle \sigma_r \rangle) \right] \tau \\ &- \kappa_s \varkappa^{-2} \langle \bar{p}_r \rangle \langle \sigma_z \rangle [1 - \cos(\varkappa\tau)] \\ &- \kappa_s \varkappa^{-3} \langle \bar{p}_r \rangle * [\sin(\varkappa\tau) - \tau] \end{aligned} \quad (14)$$

where we have defined the dimensionless coupling $\kappa = \alpha/\beta$, and the parameters $\kappa_s = 2 \left(\kappa^2 + (-1)^{1+\delta_{sy}} \right)$, $\varkappa = 2\kappa [\kappa\xi^2 + 2 \langle \bar{p}_x \bar{p}_y \rangle]$, and $\Lambda = \langle (\kappa \bar{p}_y + \bar{p}_x) \sigma_y + (\kappa \bar{p}_x + \bar{p}_y) \sigma_x \rangle$. Equation (14) shows that with both spin-orbit couplings acting together with different strengths ($\kappa \neq 1$), we still obtain similar trajectories to those coming from each coupling acting separately. Now, when considering matched coupling strengths ($\kappa = 1$, i.e., $\alpha = \beta$), two special situations arise when the electronic levels are prepared as eigenstates of σ_z or σ_s . In the first case we do not get Zitterbewegung as expected, since an eigenstate of σ_z does not simulate the superposition between positive and negative energy states required for the Zitterbewegung. However, we do obtain an interesting effect: we lock the motion of the particle in the s direction and obtain an oscillatory harmonic motion in the r direction:

$$\langle \bar{s}(\tau) \rangle = \langle \bar{s}(0) \rangle - \kappa_s \varkappa^{-2} \langle \bar{p}_r \rangle, \quad (15a)$$

$$\langle \bar{r}(\tau) \rangle = \langle \bar{r}(0) \rangle - \kappa_r \varkappa^{-2} \langle \bar{p}_s \rangle [1 - \cos(\varkappa\tau)]. \quad (15b)$$

In the second case we get a uniform motion in the s direction and the expected trembling motion in the r direction:

$$\langle \bar{s}(\tau) \rangle = \langle \bar{s}(0) \rangle + (-1)^{1+\delta_{sx}} \langle \sigma_s \rangle \tau, \quad (16a)$$

$$\begin{aligned} \langle \bar{r}(\tau) \rangle &= \langle \bar{r}(0) \rangle + (-1)^{1+\delta_{sx}} \tau \\ &- \kappa_r \varkappa^{-3} \langle \bar{p}_s \rangle \langle \bar{p}_y + \bar{p}_x \rangle [\sin(\varkappa\tau) - \tau]. \end{aligned} \quad (16b)$$

Although Eq. (16b) does not lead to trajectories similar to those discussed in Ref. [12], we note that Eq. (14) can have its parameters properly adjusted so as to produce cycloidal motion..

Ionic Lissajous trajectories. Now we revisit the anisotropic version of the Rashba-type Hamiltonian (6), $H = (\gamma_x p_x \sigma_x - \gamma_y p_y \sigma_y)$. By adjusting the laser fields such that $\gamma_y^2 \gg \gamma_x^2$ and preparing the electronic state as an eigenstate of σ_z , we obtain

$$\langle \bar{s}(\tau) \rangle = \langle \bar{s}(0) \rangle - \langle \bar{p}_r \rangle [1 - \cos(\varpi\tau)], \quad (17a)$$

$$\langle \bar{r}(\tau) \rangle = \langle \bar{r}(0) \rangle + \langle \bar{p}_s \bar{p}_r^{-1} \rangle [1 - \cos(\sqrt{\varpi}\tau)], \quad (17b)$$

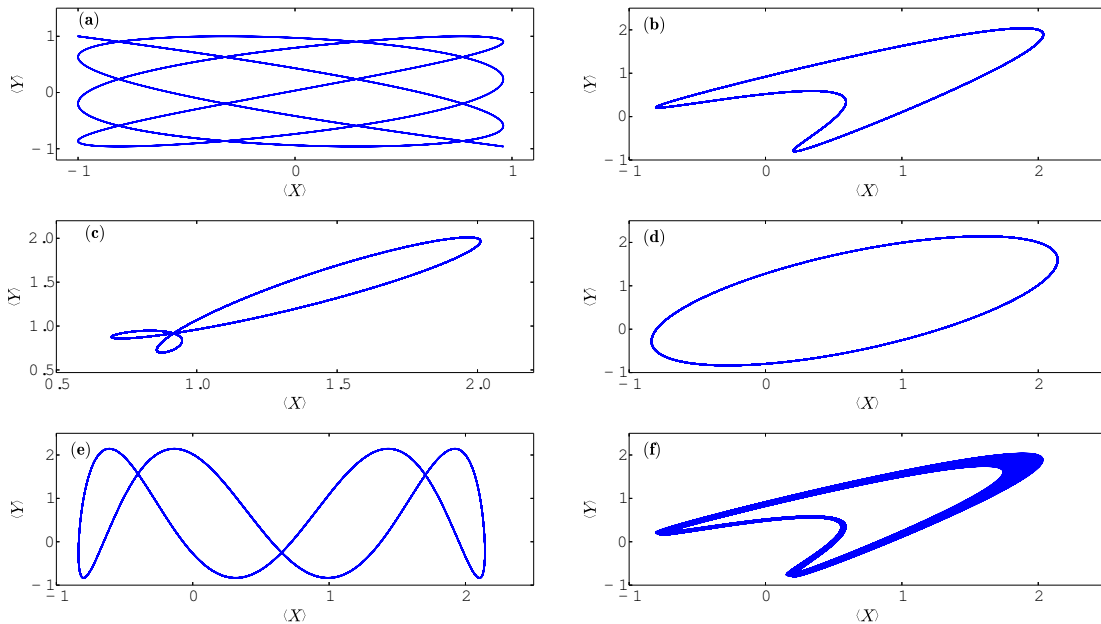


FIG. 2: (a) Lissajou curves derived from Eq. (17) with $\varpi = 1.96$ and $\eta\Omega\varpi$ and $\eta\Omega\sqrt{\varpi}$ around 50 and 35 KHz, respectively. (b) Lissajous curves numerically computed from Eq. (10), starting from initial coherent state $\Theta = 1$ and electronic levels in the superposition $|\varphi\rangle = |\uparrow\rangle - i|\downarrow\rangle$, with $N = 1$ and $\gamma_s/\Delta_s = 1$. In (c) and (d) we consider the same parameters as in (b), except for (c) $\Theta = 1 - i$ and (d) $N = 2$. In (e) we consider the same initial states as in (b) but $N = 2$, $\gamma_x/\Delta_x = 0.4$ and $\gamma_y/\Delta_y = 1$. Finally, (f) follows from the same parameters as in (b) but considering dissipative mechanisms in the vibrational degrees of freedom, with a damping rate $\zeta_s = 10^{-4}\gamma_s/\Delta_s$.

with $\varpi = (\gamma_x/\gamma_y)\langle\bar{p}_y\rangle$. In Fig. 2(a) we show Lissajous curves governed by Eq. (17) with $\varpi = 1.96$ and frequencies $\eta\Omega\varpi$ and $\eta\Omega\sqrt{\varpi}$ around 50 and 35 KHz, respectively. In this case, the Rashba energy $\gamma\sqrt{\bar{p}_x + \bar{p}_y}$ is around 10^{-10} eV. In what follows we obtain Lissajous figures from our previously introduced bounded SO interaction in Eq. (10), which requires only the preparation of an initial vibrational coherent state $|\Theta\rangle$ (differently from all the equations of motion derived above, which rely on the preparation of the initial vibrational state $|\psi(0)\rangle$). In Fig. 2(b) the mean value of the ionic position has been numerically computed (running in QuTiP [15]) from Eq. (10), with $N = 1$, $\gamma_s/\Delta_s = 1$, and starting from the vibrational mode in the coherent state $\Theta = 1$ and electronic levels in the superposition $|\varphi\rangle = |\uparrow\rangle - i|\downarrow\rangle$. In Figs. 2(c) and 2(d) we consider the same parameters as in Fig. 2(b) except for $\Theta = 1 - i$ in Fig. 2(c) and $N = 2$ in Fig. 2(d). In Fig. 2(e) we consider $N = 2$, $\gamma_x/\Delta_x = 0.4$, $\gamma_y/\Delta_y = 1$, and the same initial states as in Fig. 2(b).

Detrimental effects. To show that our calculated ionic trajectories are robust, we have included damping effects due to the environment. Figure 2(f) is similar (same parameters) to in Fig.2(b) but accounts for dissipative mechanisms in the vibrational degrees of freedom as described by the Lindbladian

$(\zeta_s/2)[2a_s\rho a_s^\dagger - a_s^\dagger a_s\rho - \rho a_s^\dagger a_s]$, with a damping rate $\zeta_s = 10^{-4}\gamma_s/\Delta_s$ [16]. Clearly, the trajectories are robust and visible for realistic parameters.

We have presented a protocol for generating Lissajous curves with the vibrational motion of an ion in a two-dimensional trap. It relies on the unique capability of our setup to realize Rashba- and Dresselhaus-type SO interactions, which allows us to simulate solid-state SO effects within a highly controllable trapped-ion experiment. We have also verified that Lissajous curves can be derived from upper-bound SO interactions, which may bring new perspectives to the subject. Addressing some interesting issues to be investigated further, we first observe that a straightforward extension to the case of many trapped ions, where the strong and tunable (up to $10^4 Hz$) SO strength can be used to explore quantum phase transitions [17] and chaotic behavior [18]. Finally, motivated by the results above, we believe it is worth to investigate the role of the ‘‘Bounded’’ spin orbit interaction in solid states systems [19].

Acknowledgements

The authors acknowledge financial support from PRP/USP within the Research Support Center Initiative (NAP Q-NANO) and FAPESP, CNPQ and CAPES,

the Brazilian agencies.

-
- [1] C. Monroe *et al.*, *Science* **272**, 1131 (1995); Q. A. Turchette *et al.*, *Phys. Rev. Lett.* **81**, 3631 (1998); C. J. Myatt *et al.*, *Nature* **403**, 269 (2000); M. A. Rowe *et al.*, *Nature* **409**, 791 (2001); M. D. Barrett *et al.*, *Nature* **429** (2004); D. Leibfried *et al.*, *Nature* **438**, 639 (2005); D. J. Wineland, *Rev. Mod. Phys.* **75**, 4714 (2013).
- [2] C. Monroe *et al.*, *Phys. Rev. Lett.* **75**, 4714 (1995); D. Kielpinski *et al.*, *Nature* **417**, 709 (2002); J. Chiaverini *et al.*, *Nature* **432**, 602 (2004); J. P. Home *et al.*, *Science* **325**, 1227 (2009); C. Ospelkaus *et al.*, *Nature* **476**, 181 (2011); J. P. Gaebler, *et al.*, *Phys. Rev. Lett.* **109**, 179902 (2012).
- [3] L. Lamata *et al.*, *Phys. Rev. Lett.* **98**, 253005 (2007).
- [4] A. Bermudez *et al.*, *Phys. Rev. A* **76**, 041801(R) (2007).
- [5] Schliemann *et al.*, *Phys. Rev. Lett.* **94**, 266801 (2005).
- [6] X. Zhang, *Phys. Rev. Lett.* **100**, 113903 (2008).
- [7] Y.-J. Lin, K. Jiménez-García, and I. B. Spielman, *Nature* **471**, 83 (2011).
- [8] J. Y. Vaishnav *et al.*, *Phys. Rev. Lett.* **100**, 153002 (2008).
- [9] L. J. Garay *et al.*, *Phys. Rev. Lett.* **85**, 4643 (2000).
- [10] K. Hamilton *et al.*, *JHEP* **10**, 222 (2013); F.-J. Huang, Q.-H. Chen, W.-M. Liu, arXiv:1207.3707v3 [cond-mat.quant-gas] (2013).
- [11] R. Gerritsma *et al.*, *Nature* **463**, 68 (2010).
- [12] E. Bernardes *et al.*, *Phys. Rev. Lett.* **99**, 076603 (2007).
- [13] C. A. Sackett *et al.*, *Nature (London)* **404**, 256 (2000).
- [14] R. F. Rossetti *et al.*, *Phys. Rev. A* **90**, 033840 (2014).
- [15] J. R. Johansson, P. D. Nation, and F. Nori, *Comput. Phys. Commun.* **183**, 1760 (2012); *ibid.* **184**, 1234 (2013).
- [16] D. Leibfried *et al.*, *Rev. Mod. Phys.* **75**, 281 (2003).
- [17] Y. Zhang, G. Chen, and C. Zhang, *Sci. Rep.* **3**, 1937 (2013).
- [18] J. Larson, B. M. Anderson, and A. Altland; *Phys. Rev. A* **87**, 013624 (2013).
- [19] I. Zutic, J. Fabian and S. Das Sarma, *Rev. Mod. Phys.* **76**, 323 (2004).